Acta Pharmacologica Sinica (2017) 38: 848–858
www.nature.com/aps

Open

Original Article

Self-assembled nanocomplex between polymerized phenylboronic acid and doxorubicin for efficient tumor-targeted chemotherapy

Junseok LEE[1, #], Jinhwan KIM[1, 2, #], Yeong Mi LEE[2], Dongsik PARK[2], Sooseok IM[3], Eun Ho SONG[2], Hansoo PARK[4], Won Jong KIM[1, 2, 3, *]

[1]Center for Self-assembly and Complexity, Institute of Basic Science (IBS), Pohang 37673, Republic of Korea; [2]Department of Chemistry, Pohang University of Science and Technology (POSTECH), Pohang 37673, Republic of Korea; [3]School of Interdisciplinary Bioscience and Bioengineering, Pohang University of Science and Technology (POSTECH), Pohang 37673, Republic of Korea; [4]School of Integrative Engineering, Chung-Ang University, Seoul 156–751, Republic of Korea

Abstract

Since the discovery that nano-scaled particulates can easily be incorporated into tumors via the enhanced permeability and retention (EPR) effect, such nanostructures have been exploited as therapeutic small molecule delivery systems. However, the convoluted synthetic process of conventional nanostructures has impeded their feasibility and reproducibility in clinical applications. Herein, we report an easily prepared formulation of self-assembled nanostructures for systemic delivery of the anti-cancer drug doxorubicin (DOX). Phenylboronic acid (PBA) was grafted onto the polymeric backbone of poly(maleic anhydride). pPBA-DOX nanocomplexes were prepared by simple mixing, on the basis of the strong interaction between the 1,3-diol of DOX and the PBA moiety on pPBA. Three nanocomplexes (1, 2, 4) were designed on the basis of [PBA]:[DOX] molar ratios of 1:1, 2:1, and 4:1, respectively, to investigate the function of the residual PBA moiety as a targeting ligand. An acid-labile drug release profile was observed, owing to the intrinsic properties of the phenylboronic ester. Moreover, the tumor-targeting ability of the nanocomplexes was demonstrated, both *in vitro* by confocal microscopy and *in vivo* by fluorescence imaging, to be driven by an inherent property of the residual PBA. Ligand competition assays with free PBA pre-treatment demonstrated the targeting effect of the residual PBA from the nanocomplexes 2 and 4. Finally, the nanocomplexes 2 and 4, compared with the free DOX, exhibited significantly greater anti-cancer effects *in vitro* and even *in vivo*. Our pPBA-DOX nanocomplex enables a new paradigm for self-assembled nanostructures with potential biomedical applications.

Keywords: doxorubicin; anticancer drugs; nano-sized complex; boronic ester; pH-responsive; self-assembly

Acta Pharmacologica Sinica (2017) 38: 848–858; doi: 10.1038/aps.2017.16; published online 17 Apr 2017

Introduction

Self-assembly is a natural process in which disordered components are spontaneously assembled into a certain structure or pattern[1]. Non-covalent interactions such as hydrogen bonding, van der Waals interactions, and electrostatic interactions are major driving forces of self-assembly[2–4]. In particular, nano-sized and self-assembled structures are one of the most useful materials to provide various functionalities in biomedical applications[5–8]. For instance, the nano-sized and self-assembled structures are highly useful for the delivery of hydrophobic anti-cancer drugs because of their facile formulation. In addition, these structures exhibit the unique property of accumulating within the tumor site because of their enhanced permeability and retention (EPR) effect[9–13]. Therefore, various formulations such as liposomes, polymeric micelles, polymersomes, and inorganic-organic hybrids have been developed and evaluated over the course of decades for use in biomedical applications[14–18]. Doxorubicin (DOX) is a one of the most commonly used anti-cancer chemotherapeutics for various types of cancer, including blood, breast, lung, and ovarian cancers[19–22]. The molecular structure of DOX comprises two characteristic parts: the hydrophobic tetracycline ring and an amine-functionalized sugar. Although DOX is administered intravenously as an aqueous solution of the hydrochloride salt, several studies have reported hemolytic activity of DOX, resulting from its cationic charge and hydrophobicity[23–25]. To improve the blood compatibility of

# These authors contributed equally to this work.
*To whom correspondence should be addressed.
E-mail wjkim@postech.ac.kr
Received 2016-11-20 Accepted 2017-02-20

DOX and extend its circulation time in the blood, liposomal formulations have been introduced and recently commercialized, including Doxil®, Myocet®, and Caelyx® [26–29]. However, there are concerns about non-specific leakage from liposomes and polymeric micelles during blood circulation, which can be driven by large dilution and decreased stability under high salt conditions. Therefore, a more stable nanoparticle system is still needed for the efficient delivery of DOX to enhance the drug's efficacy and limit its side effects[30–32]. In that regard, the distinct chemical features of DOX, such as its hydrophobicity and cationic charge, have been exploited for loading DOX into delivery cargos such as the hydrophobic core of liposomes, polymeric micelles, or nanoparticles[18, 33–37]. Further, DOX has been adsorbed on the surface of carbon nanomaterials and intercalated into specific DNA sequences *via* π-π interaction[17, 38–41]. Charge interaction with negatively charged materials such as the surface of silica or polyanions is another common strategy utilized for loading DOX[42, 43]. However, such systems impede the precise control of drug loading, and complicated chemical modification is required in many cases. Here, we approached this issue from a different direction from the approaches used in previous studies. The molecular structure of DOX contains a 9-(2-hydroxyacetyl) group and the 9*S*-hydroxyl group, which comprise a 1,3-diol conformation. Notably, phenylboronic acid (PBA) has a remarkable binding affinity toward 1,2-*cis*-diols and 1,3-diols *via* the formation of a boronic ester[44–47]. Therefore, strong binding between PBA and DOX was expected and provided clues to a new strategy for formulatinge self-assembled nanostructures.

Recently, our group has reported the self-assembled architecture between PBA-grafted polyethyleneimine (PEI) and sugar-grafted PEI *via* the formation of a phenylboronic ester, and has found that the resultant products exhibit feasible gene delivery efficacy[48]. We have also reported nanocomplexes of entangled poly-paclitaxel (pPTX) and poly-cyclodextrin (pCD) via the self-assembly of a CD::PTX inclusion complex for the enhanced aqueous solubility and delivery of PTX[40]. Extending our previous studies, here we developed a nanocomplex between polymerized PBA (pPBA) and DOX and evaluated that nanocomplex both *in vitro* and *in vivo*. PBA was grafted onto the backbone of poly(maleic anhydride) by a spontaneous ring opening reaction to achieve pPBA. Because neither catalysts nor toxic organic solvents were utilized, the synthetic strategy of pPBA demonstrated atom economy and green chemistry[49]. Through the simple process of mixing aqueous solutions of pPBA and DOX, self-assembled pPBA-DOX nanocomplexes were generated via the hydrophobic interaction between the PBA-DOX pairs. Furthermore, DOX was easily released at the intracellular pH, owing to the pH sensitivity of the boronic ester, and further destruction was observed (Scheme 1). A remarkable therapeutic effect is expected from our rationally designed pPBA-DOX nanocomplexes both *in vitro* and *in vivo*: because 1) the circulation time *in vivo* can be extended by blocking non-specific interactions with blood components, owing to the negative charge from the residual carboxylic group, 2) the suitable size of the nanocomplexes enables effective tumor accumulation *via* the EPR effect *in vivo*, 3) the remaining PBA moieties can be exploited as a tumor-targeting ligand, and 4) DOX can be released in response to the intracellular environment. Consequently, a simple but efficient pPBA-DOX nanocomplex would provide a fascinating strategy for the delivery of conventional drugs not only in anti-cancer therapy but also in broader treatment methods.

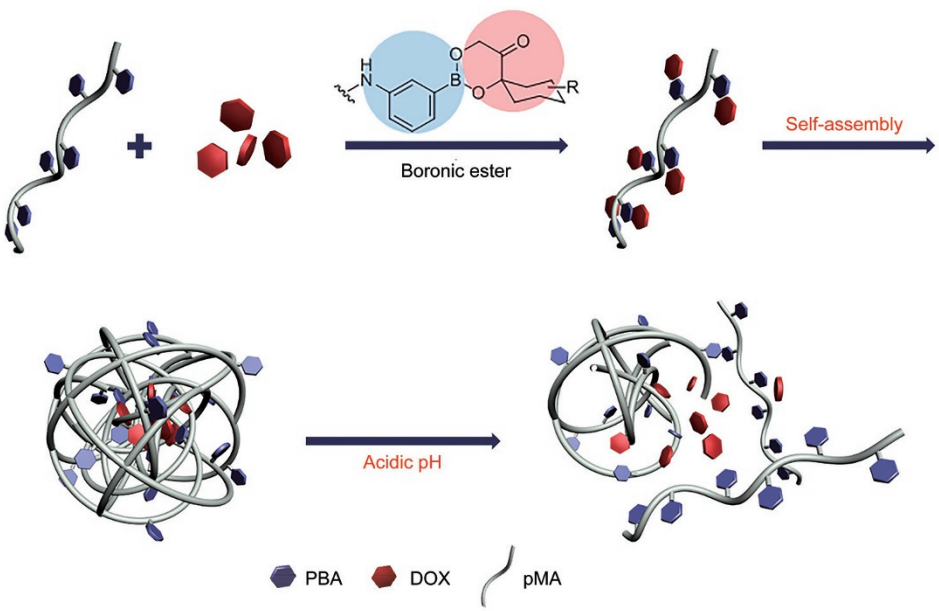

Scheme 1. Schematic illustration for formulation and destruction of pPBA-DOX nanocomplex. Formulation of nanocomplex is driven by charge interaction and the boronic ester formation between phenylboronate of pPBA and 1,3-diol of DOX. At an acidic pH, destruction of nanocomplex is induced by decreased affinity of boronic ester, and finally DOX is released.

Materials and methods

Reagents

Poly(methyl vinyl ether-*alt*-maleic anhydride) (pMA; M_n ~80 000 g/mol), 3-aminophenylboronic acid (PBA-NH_2) monohydrate, and thiazolyl blue tetrazolium bromide (MTT) were purchased from Sigma-Aldrich (St Louis, MO, USA). FCR648-NH_2 was purchased from BioActs (Korea). Doxorubicin (DOX) was purchased from Wako Chemical (Japan). All reagents were used as received without further purification.

Instrumental methods

Transmission electron microscopy (TEM) images were taken using a transmission electron microscope (JEM-2210, JEOL) and analyzed using Gatan DigitalMicrograph software. UV-vis absorbance for the MTT assay was measured using a microplate spectrofluorometer (VICTOR3 V multilabel counter), and fluorescence spectra were obtained from a spectrofluorophotometer (RF-5301 PC, Shimadzu) or multi-well plate reader (SpectraMax® i3, Molecular Devices). Hydrodynamic size and zeta potential were measured using a Zetasizer (Nano S90, Nano Z, respectively; Malvern) at 0.1 mmol/L in Dulbecco's phosphate-buffered saline (DPBS, pH 7.4) or 0.1 mol/L acetate buffer (pH 5.5). The confocal laser scanning microscope (CLSM) images were obtained using an Olympus FV-1000 and analyzed using the Olympus FluoView ver 1.7 software.

Preparation of poly(phenylboronic acid-co-maleic anhydride) (pPBA)

PBA-conjugated pMA (pPBA) was prepared by spontaneous amide coupling of the acid anhydride moiety onto the pMA backbone and -NH_2 of PBA-NH_2 *via* a ring opening reaction (Scheme S2). Briefly, 500 mg of pMA (3.2 mmol anhydride eq) and 160 mg of PBA-NH_2 (1 mmol) were dissolved in 15 mL of dry dimethyl sulfoxide (DMSO) and stirred at room temperature (RT) overnight. Unreacted succinic anhydride moieties were hydrolyzed by adding 10 mL of 0.1 mol/L NaOH and dialyzed against deionized water for two days (molecular weight cut-off=10 000), followed by lyophilization. The molar ratio of conjugated PBA was calculated by ^{1}H NMR (yield: 91%). ^{1}H NMR (D_2O, 300 MHz): 7.7–7.0 (m, *Ph*, 4*x*H); 3.8–3.5 (m, –C*H*–, 1H); 3.5-3.1 (m, –OCH_3, 3H); 3.1–2.4 (m, anhydride, 2H); 2.4–1.4 (m, –CH_2–, 2H).

For various imaging experiments *in vitro* and *in vivo*, red fluorescence dye was conjugated onto the pPBA backbone in the same manner. In brief, 200 mg of pMA, 70 mg of PBA-NH_2, and 5 mg of FCR648-NH_2 were fully dissolved in 15 mL of dry DMSO and stirred at RT overnight. Then, 10 mL of 0.1 mol/L NaOH was added and dialyzed against water for two days (molecular weight cutoff=10 000), and this was followed by lyophilization. The conjugation ratio of PBA was calculated from the ^{1}H NMR (yield: 95%).

As a control polymer that contains no PBA moiety, pMA was hydrolyzed by NaOH and dissolved in DPBS to obtain hydrolyzed poly(maleic anhydride) (pMAh) solution. For the controlled experiment, [COO^-] from the hydrolyzed succinic anhydride subunit was equalized from both pPBA and pMAh solutions.

Formulation of pPBA-DOX nanocomplexes

The pPBA-DOX nanocomplexes were simply prepared by mixing the pPBA and DOX solutions. For nanocomplexes with [PBA]:[DOX] molar ratios of 1:1, 2:1, or 4:1 (nanocomplexes 1, 2, and 4, respectively) containing 2 mmol/L DOX equivalent, 200 μL of 10 mmol/L DOX was added into 100, 200, or 400 μL of 20 mmol/L pPBA, respectively. Then, 100 μL of 10× PBS (pH 7.4) was added to the solution, and the vial was filled to 1 mL with deionized water. For the quenching assay, pPBA was fixed at 1 mmol/L, and the amount of DOX varied. For the quenching assay of DOX, DOX was fixed at 1 mmol/L, and the amount of pPBA varied. For the formulation of dye-labeled nanocomplexes, non-labeled pPBA and FCR648-labeled pPBA were mixed at the ratio of 1:1 and 1:3 for the formulation of nanocomplexes 2 and 4, respectively, to normalize the fluorescence intensity.

Stimuli-responsive drug release

Drug release from nanocomplexes 1, 2, and 4 at pH 7.4 and 5.5 was monitored by the inherent fluorescence of DOX (E_x=495 nm, E_m=590 nm). Within a desired time interval, the solution was centrifuged (13 500 r/min, 5 min), and the fluorescence of the supernatant was measured. The amount of released DOX was calculated as [(released drug)/(loaded drug)×100].

In vitro cell viability test

To evaluate the therapeutic efficiency of the nanocomplexes, the cytotoxicity of the nanocomplexes or control samples was measured with MTT assays. Cells (human breast cancer cells, MCF-7 and human prostate cancer cells, PC-3) were seeded on a 96-well culture plate at a density of 8000 cells/well and incubated overnight. Fresh medium was treated with either pPBA at a final concentration of 0 to 40 μmol/L, free DOX, or nanocomplexes 1, 2, and 4 at a final equivalent DOX concentration of 0 to 10 μmol/L. The medium was then incubated with the cells for another 48 h. After incubation, the cell viability was evaluated with MTT assays.

For the MTT assays, cells were washed with DPBS, and the medium was replaced with 200 μL of MTT solution in the medium (0.5 mg/mL). After incubation in the dark for 4 h, the medium was removed thoroughly, and purple crystals were completely dissolved by 200 μL of DMSO. Each sample (100 μL) was transferred into a new 96-well plate, and UV-vis absorbance was measured at 570 nm using a microplate spectrofluorometer (VICTOR3 V multilabel counter). The relative percentages of non-treated cells were used to represent 100% cell viability.

Competition assay *in vitro*

The PBA-mediated uptake of nanocomplexes was evaluated with competitive assays. Cells (MCF-7 or PC-3) were seeded on a 96-well culture plate at a density of 8000 cells/well and

incubated overnight. After being washed with DPBS, the cells were incubated with pre-treated serum-free medium with or without 5 mmol/L PBA-NH_2 for 30 min. Then, cells were washed and incubated with serum-free medium treated with 0 to 40 μmol/L pPBA, free DOX, or nanocomplexes 1, 2, and 4 at a final equivalent DOX concentration of 0 to 10 μmol/L for 4 h. Cells were washed and further incubated for 44 h, then the cell viability was measured with MTT assays.

Intracellular uptake of nanocomplexes by confocal laser scanning microscopy (CLSM)

The intracellular uptake of nanocomplexes with or without competitor was analyzed by confocal microscopy imaging. Briefly, MCF-7 or PC-3 cells (100 000 cells/well) were seeded on glass coverslips placed in a 12-well culture plate. Cells were incubated overnight and incubated for 30 min with pre-treated serum-free medium with or without 5 mmol/L PBA-NH_2 as a competitor. Then, the medium was replaced with fresh serum-free medium containing 2 μmol/L DOX equivalent of pPBA or nanocomplexes 1, 2, and 4 and further incubated for 4 h. To observe the localization of pPBA, FCR648-labeled pPBA was incorporated and diluted with pPBA to control the fluorescence intensity. Cells were washed with DPBS and fixed immediately with 10% neutrally buffered formalin at 4 °C overnight. Cells on the coverslips were mounted with Vectashield anti-fade mounting medium containing 4′,6-diamidine-2′-phenylindole dihydrochloride (DAPI) (Vector Labs). The intracellular fluorescence of pPBA-FCR648 and DOX was observed by CLSM at excitation/emission wavelengths of 633/647 and 488/530 nm, respectively.

Hemolysis assay

Hemolysis of each sample was evaluated by measuring the released hemoglobin from the erythrocytes. Briefly, fresh mouse blood was prepared in a heparin tube and diluted tenfold by DPBS, and this was followed by centrifugation (2000 r/min, 15 min) to isolate the red blood cells (RBCs). RBCs were diluted, and samples (pPBA, DOX, nanocomplexes 1, 2, and 4) were added with a final concentration of 1 mmol/L DOX equivalent. The suspensions were incubated at 37 °C for 4 h and then centrifuged (2000 r/min, 15 min) to separate the RBC pellet. The absorbance of the supernatant at 400 nm was measured to minimize the absorbance of released DOX and maximize the absorbance of hemoglobin. Saline and 1× lysis buffer were considered to represent 0 and 100% hemolysis, respectively.

In vivo biodistribution of pPBA-DOX Nanocomplexes

All animal experiments were approved by the POSTECH Biotech Center Ethics Committee. CT-26 cells (1 000 000 cells/mouse) were inoculated subcutaneously (sc) into the flanks of female Balb/c mice. After the average tumor volume reached approximately 300 mm^3, saline, FCR648-labeled pPBA, nanocomplexes 1, 2, and 4 (3 mg/kg DOX) were systemically injected. Nanocomplexes 2 and 4 were formulated with the same molar ratio of FCR648-labeled pPBA and the rest with non-labeled pPBA to normalize the fluorescence signal. At 24 h post-injection, the fluorescence intensities of the mice and tumors were measured with an IVIS spectrum small-animal *in vivo* imaging system at Pohang Technopark Biotech Center (Califer Lifescience, Hopkinton, MA, USA). For the *ex vivo* imaging of DOX, saline, free DOX, and nanocomplex 4 (3 mg/kg) were injected, and the epifluorescence of DOX from the tumor was compared using IVIS imaging in the same manner.

Anti-tumor study in a mouse model

CT26/FLuc cells (1 000 000 cells/mouse) were inoculated *sc* into the flanks of female Balb/c mice. When the average tumor volume reached approximately 300 mm^3, the mice were divided randomly into 6 groups (7 mice per group). The mice were then injected with 200 μL of each sample: 1) saline, 2) pPBA, 3) free DOX, 4) nanocomplex 1, 5) nanocomplex 2, and 6) nanocomplex 4 (3 mg/kg DOX at d 0 and 4), and the tumor volume was monitored every day after the systematic injection of the samples. Tumor volumes were recorded following the equation for a prolate ellipsoid of $ab^2/2$, where a is the longest and b is the shortest dimension. Tumor growth was monitored until the tumor was ulcerated, at which time the mice were sacrificed according to the rules of the POSTECH Biotech Center Ethics Committee. All data were represented as the mean±SEM, and all significant differences were analyzed with OriginPro 8. The tumor inhibition rate was calculated as the ratio between the final and initial volumes of the tumor. Perfect tumor inhibition (100%) was set as total growth regression, and 0% tumor inhibition was set as the growth rate of the saline-treated group. For imaging the tumor, luciferin substrate was injected intraperitoneally immediately before *in vivo* imaging, and the luminescence of the tumor was imaged after 10 min. The image was obtained and analyzed with IVIS.

Results

Preparation and characterization of pPBA

Briefly, polymerized PBA (pPBA) was synthesized by chemical conjugation between 3-aminophenylboronic acid (PBA-NH_2) and poly(maleic anhydride) (pMA). The conjugation ratio was 156 PBA moieties per 513 maleic anhydride subunits, as calculated by ^{1}H NMR from the ratio between the aromatic region of PBA and –CH_2– of the polymer backbone (Figure S1). The Fourier transform infrared spectra of pMA and pPBA also indicated the successful conjugation of PBA and the hydrolysis of the anhydride, which were represented by the disappearance of the acid anhydride peaks (1830–1800 cm^{-1} and 1775–1740 cm^{-1}) and the appearance of both carboxylic acid (1730–1700 cm^{-1}) and amide (1680–1630 cm^{-1}) of pPBA (Figure S2)[50].

Preparation and characterization of the pPBA-DOX nanocomplexes

For the next step, pPBA-DOX nanocomplexes were readily prepared by simple mixing, on the basis of the strong interaction between the 1,3-diol of DOX and the PBA moiety

on pPBA. Three different nanocomplexes (1, 2, and 4) were designed on the basis of molar ratios of 1:1, 2:1, and 4:1 (PBA to pPBA:DOX), respectively, to investigate the function of the residual PBA moiety as a targeting ligand. The sizes of the nanocomplexes were measured at the sub-hundred nanometer scale (Figure 1A). As a control, hydrolyzed pMA (pMAh) was mixed with DOX, thus resulting in severe aggregation and precipitation and indicating that the PBA-diol interaction is a major driving force in the formation of the nanocomplexes (Figure S3). To further validate the formation of boronic ester, the fluorescence of pPBA was measured, because the steady-state quenching of the inherent fluorescence of PBA is induced by the formation of the boronic ester[48]. The boronic ester was quantitatively formed by mixing pPBA with DOX, thus suggesting that residual PBA moieties exist and may have functioned as a targeting ligand (Figure S4A). In addition, the formation of the hydrophobic core was demonstrated by the fluorescence of DOX because DOX fluorescence is quenched by π–π stacking[34]. As expected, noticeable quenching of the DOX fluorescence was observed, thereby suggesting π-π stacking of DOX at the hydrophobic core of the nanocomplexes (Figure S4B).

pH-responsive properties of nanocomplexes

Because the phenylboronic ester linkage shows pH-sensitive behavior, pH-responsive drug release and structural deformation of the nanocomplexes were expected (Scheme S3). At a neutral pH, all three nanocomplexes exhibited a hydrodynamic size of approximately 80 nm, whereas the size distribution increased to approximately 200 nm at an acidic pH (Figure 1A). In addition, TEM imaging confirmed that the condensed structure of nanocomplexes 1, 2, and 4 at neutral pH was deformed at acidic pH, corresponding to the data obtained from dynamic light scattering (Figure 1C, 1D, S3C-D).

Given the change in size distribution, the pH-responsive drug release profile of pPBA-DOX nanocomplexes was measured at pH 7.4 and 5.5 (Figure 1B). At endosomal pH, all three nanocomplexes showed 70%–80% drug release in 24 h. In contrast, 20%, 40%, and 30%, respectively, were released from nanocomplexes 1, 2, and 4 at physiological pH. Interestingly, nanocomplexes 2 and 4 were less pH-responsive, in contrast to the dramatic pH-responsive release of nanocomplex 1, probably as a result of a combinatorial effect of increased charge interaction between the carboxylic group on the pMA backbone and DOX as well as the increased hydrophobicity of pMA at acidic pH (Figure S5B).

In vitro cytotoxicity and tumor targeting

The cytotoxicity of the materials was evaluated *in vitro* to demonstrate the therapeutic effect of the nanocomplexes (Figure 2). The toxicity of pPBA was negligible because of the highly

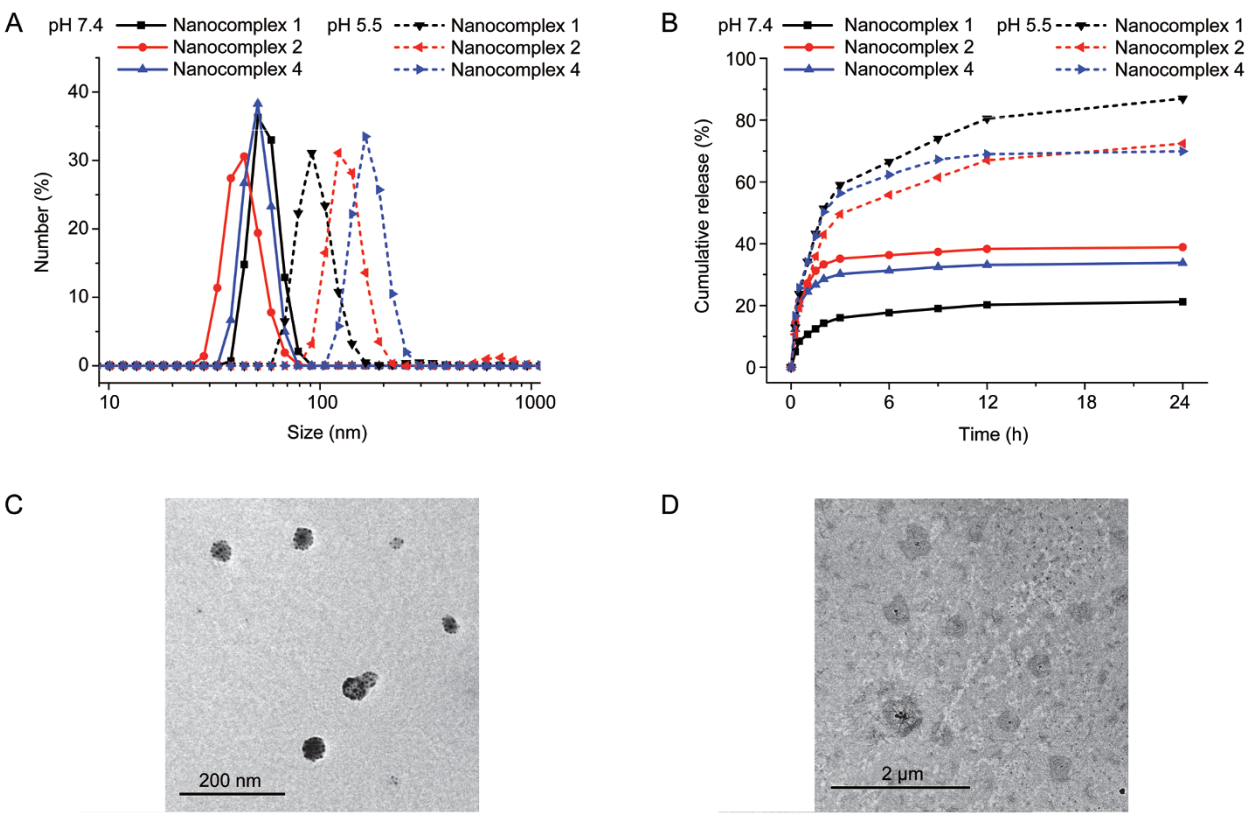

Figure 1. Physicochemical characterization of nanocomplexes. (A) Size distribution of nanocomplex 1, 2 and 4. (B) Drug release profile of nanocomplex 1, 2 and 4 at pH 7.4 and 5.5. TEM images of nanocomplex 4 at (C) pH 7.4 and (D) pH 5.5.

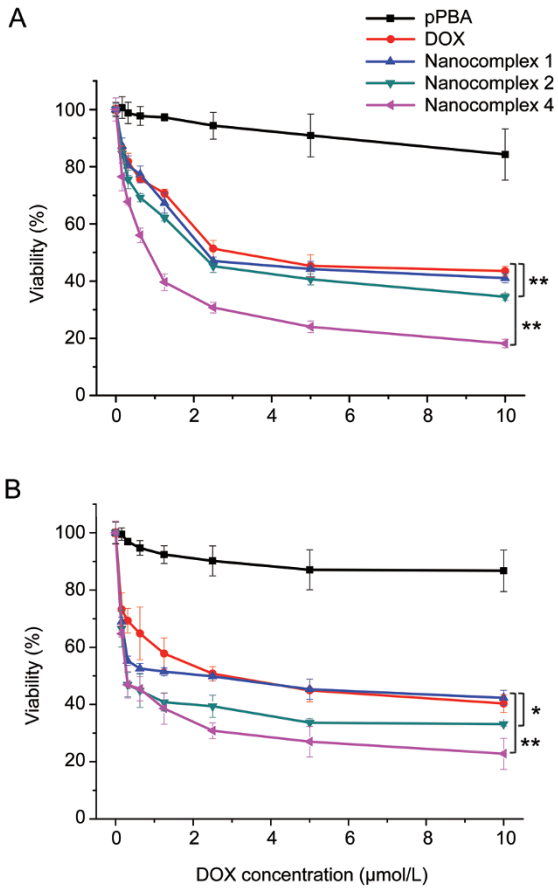

Figure 2. *In vitro* cytotoxicity of pPBA, DOX, nanocomplex 1, 2 and 4 studied in (A) MCF-7 and (B) PC-3 cell line. $^{*}P<0.05$, $^{**}P<0.01$.

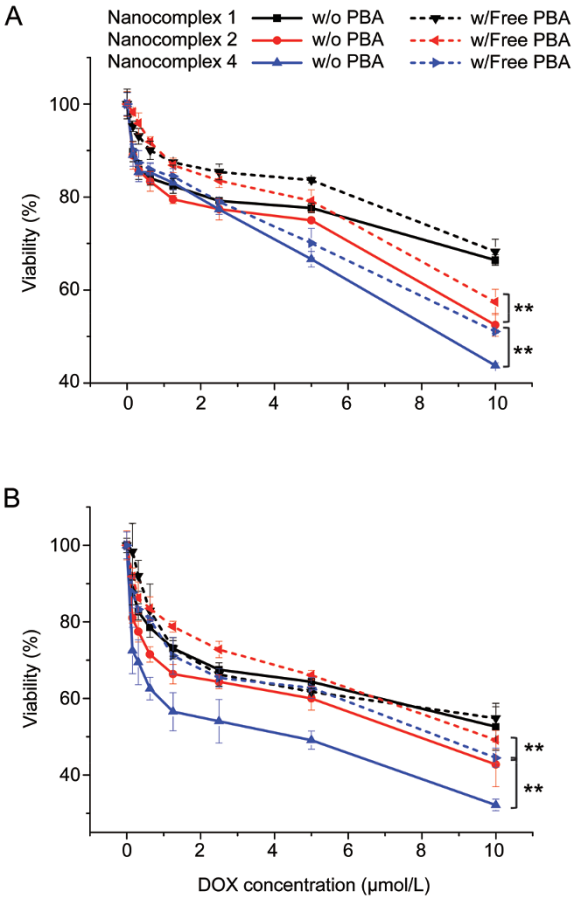

Figure 3. Competition assay *in vitro*. Cytotoxicity of nanocomplex 1, 2 and 4 studied in (A) MCF-7 and (B) PC-3 cell line with or without pre-treatment of PBA-NH_2. $^{**}P<0.01$.

negative charge of the polymer backbone and biocompatibility (Figure S5B). In the MCF-7 human breast cancer cell line, the IC_{50} value of free DOX was measured as 3.1 μmol/L, and the IC_{50} values of nanocomplexes 1 and 2 were 2.3 and 2.1 μmol/L, respectively (Figure 2A). Surprisingly, nanocomplex 4 exhibited an IC_{50} value of 0.85 μmol/L DOX equivalent, which was 3.6-fold more effective than that of free DOX and was possibly due to the targeting effect of the residual PBA moieties. Similar results were observed in the PC-3 human prostate cancer cell line (Figure 2B).

To verify the targeting effect of the residual PBA from nanocomplexes 2 and 4, ligand competition assays were conducted. As expected, the toxicity of pPBA and DOX was not affected by pre-treatment with PBA (Figure S6). In addition, the cytotoxicity of nanocomplex 1 was not influenced by additional ligands, whereas the cytotoxicity of nanocomplexes 2 and 4 decreased significantly with the pre-treatment of the free ligands (Figure 3).

To further investigate the PBA-mediated uptake, confocal microscopy images were taken with or without pre-treatment of free PBA. For quantitative microscopic imaging, some portions of pPBA were replaced by FCR648-labeled pPBA (FCR648-pPBA), and the fluorescence per nanocomplex was equalized with the addition of non-labeled pPBA. As expected, the cellular uptake of nanocomplex 4 was mostly inhibited by the pre-treatment with free PBA, corresponding to the cytotoxic effect observed in the competition assay (Figures 4, S7, and S8). In addition, the uptake of pPBA was not significantly affected by competitive inhibitors, thus indicating that the formation of a condensed structure is an effective factor for efficient uptake (Figure S9).

In vivo tumor targeting

Before evaluation of the anti-tumor effect of the nanocomplexes *in vivo*, the blood compatibility of the nanocomplexes was evaluated by hemolysis assays (Figure S10). Significant hemolysis was induced by free DOX, whereas none of the pPBA materials exhibited hemolysis, owing to their negative charge.

Given that the *in vitro* targeting ability of pPBA materials was confirmed, the *in vivo* biodistribution was next determined to demonstrate the targeting effect of the nanocomplexes. FCR648-pPBA (4 mmol/L) or FCR648-labeled nanocomplexes of 1 mmol/L DOX equivalence were systemically injected, and their distribution was observed after 24 h by whole-

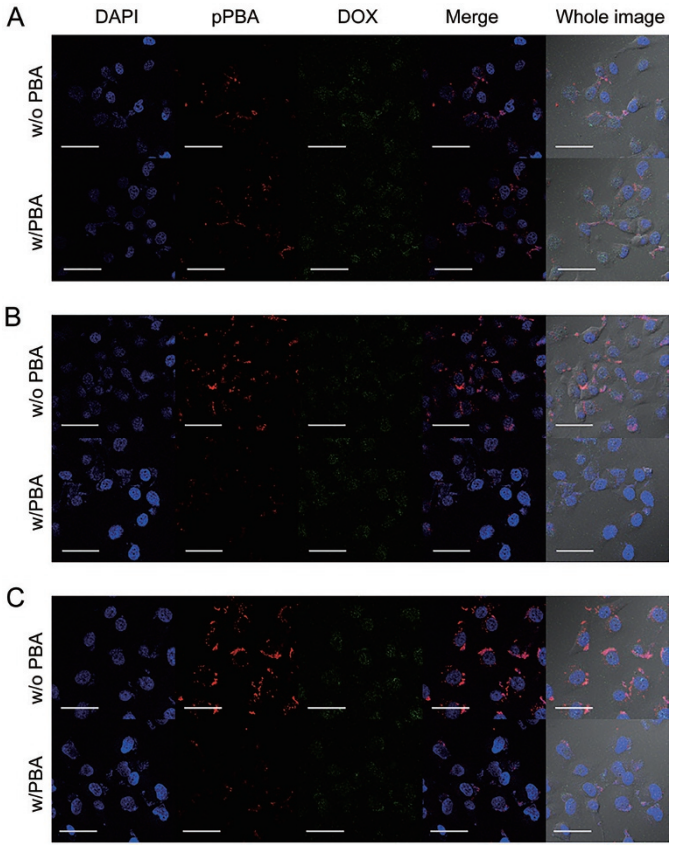

Figure 4. Competition assay *in vitro*. (A) Nanocomplex 1, (B) nanocomplex 2 and (C) nanocomplex 4-treated MCF-7 cell line with or without pre-treatment of PBA-NH_2 were analyzed by confocal microscopy. Blue images represent nucleus, red images represent pPBA in nanocomplexes, and green images represent DOX.

body fluorescence imaging (Figure 5). The accumulation of nanocomplexes was significantly enhanced as the amount of residual pPBA was increased. Quantitatively, nanocomplex 4 exhibited a 2.5-fold stronger signal from the tumor region than did nanocomplex 1. In addition, most of the fluorescence signal from the pPBA-injected mice was observed at the kidney. Similarly, *ex vivo* images of each tumor showed significant contrast in the epifluorescence (Figure 5B and 5D). Furthermore, an accumulation of DOX was detected by *ex vivo* imaging of the tumor site, and a higher level of DOX was observed in the tumor treated with nanocomplex 4 h than in the tumor treated with free DOX (Figure S11).

In vivo anti-tumor effect

To evaluate the therapeutic effect of pPBA-DOX nanocomplexes *in vivo*, tumor growth in CT26/FLuc-inoculated allograft mice was monitored after the injection of saline, pPBA, free DOX, and nanocomplexes 1, 2, and 4 (3 mg/kg DOX equivalent) at days 0 and 4 (Figure 6A). The tendencies for tumor growth between saline- and pPBA-injected mice were similar, and certain levels of anti-tumor effect were observed in mice treated with DOX and nanocomplex 1. As expected, nanocomplexes 2 and 4 exhibited the most significant anti-tumor effect, as compared with the other samples. In addition, none of the treated groups showed abrupt changes in body weight (Figure S12A).

After monitoring of the tumor growth, the viability of the grown tumor was evaluated by assessing the inherent luciferase expression of CT26/FLuc (Figure 6B and 6C). The luciferase activity in the CT26/FLuc tumor was significantly diminished in mice treated with nanocomplexes 1 to 4. In

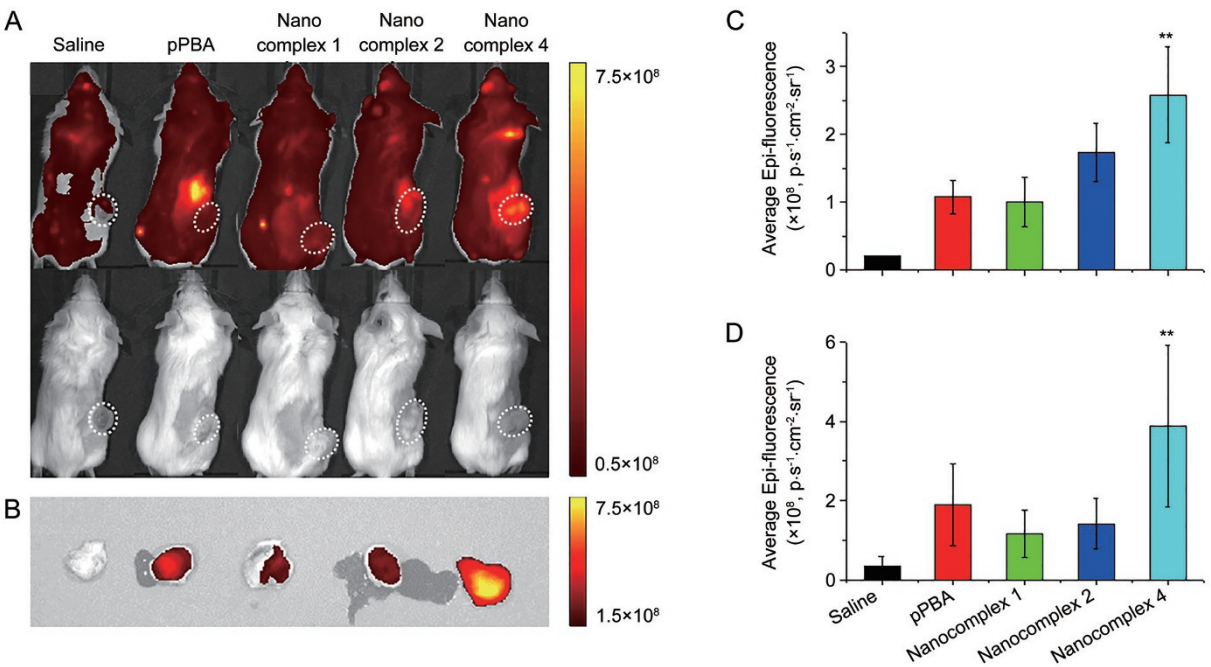

Figure 5. (A) *In vivo* bio-distribution of saline, pPBA, nanocomplex 1, 2 and 4 after 24 h injection and (B) *Ex vivo* images of corresponding tumors. The average epi-fluorescence from (C) *in vivo* nanocomplexes treated tumor site and (D) *ex vivo* corresponding tumors. $^{**}P<0.01$ *vs* Nanocomplex 1.

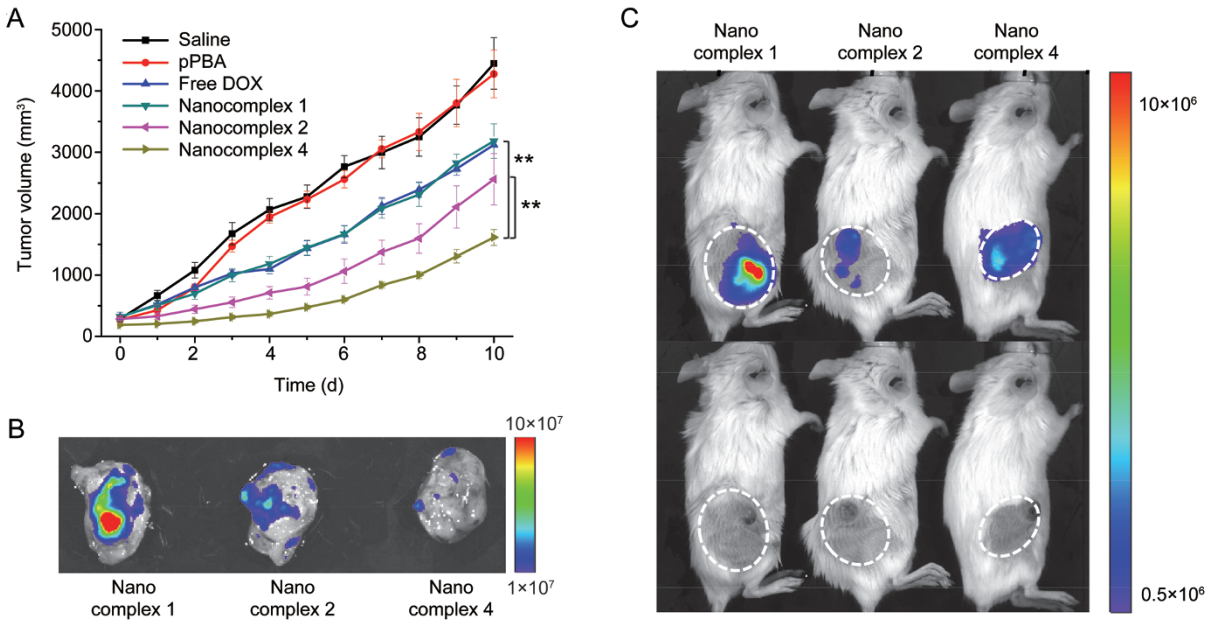

Figure 6. *In vivo* anti-tumor study. (A) Tumor growth of CT26/FLuc bearing Balb/c mice. Error bars represent±SEM. n=7. $^{**}P$<0.01. (B) Representative luminescence image from CT26/FLuc tumor of nanocomplex 1, 2 and 4 injected mice and (C) corresponding *ex vivo* image.

agreement with previous *in vitro* and *in vivo* results, the luciferase activities in the tumors from saline- and pPBA-treated mice were similar, whereas the luciferase activity in the DOX-treated group declined significantly (Figure S12C).

Discussion

Drug delivery systems using nano-sized complexes have been developed to improve the aqueous stability of drug molecules and to enhance their accumulation at the tumor site via the EPR effect. For higher efficacy and clinical translation, the nanocomplexes need to be conveniently formulated, to be stable during blood circulation and to be able to internalize target sites, specifically by using targeting ligands. In most cases, however, complicated chemical modifications are required to achieve the criteria mentioned above, thus limiting the reproducibility of results for clinical translation. In this study, the binding of PBA with DOX through their chemical structures provides a simple strategy not only for the formulation of nanocomplexes but also for the targeted delivery system.

From that perspective, we formulated tumor-targeting self-assembled nanocomplexes, using polymerized PBA and DOX. Briefly, polymerized PBA (pPBA) was synthesized by simple mixing of 3-aminophenylboronic acid (PBA-NH_2) and poly(maleic anhydride) (pMA) *via* the spontaneous ring opening reaction of the succinic anhydride moiety, and this was followed by hydrolysis of the remaining anhydride moieties to obtain carboxylic acids. In the next step, pPBA-DOX nanocomplexes were formulated through simple mixing by exploiting the interaction between the 1,3-diol of DOX and the PBA moiety on pPBA. Both passive targeting by proper size (50–200 nm) measured by dynamic light scattering and active targeting by the PBA moiety, which has high binding affinity to sialylated epitopes on tumor cells, were expected[51–53]. To verify the formation of nanocomplexes from the formation of a phenylboronic ester, hydrolyzed pMA (pMAh) was mixed with DOX in the same manner as in the control group. A clear nanocomplex solution was achieved from the pPBA group, whereas severe aggregation and precipitation were observed in all nanocomplexes formulated by pMAh, thus indicating that the PBA-diol interaction is a major driving force in the formation of the nanocomplexes.

As previously mentioned, the formation of a phenylboronic ester bond is highly responsive to environmental pH. The ester bond is particularly labile at acidic pH, such as that in the endosomal environment, whereas the bond itself is stable under physiological conditions. Therefore, a pH-responsive drug release and structural deformation of nanocomplexes were expected. At neutral pH, all three nanocomplexes exhibited a hydrodynamic size of approximately 80 nm, which is suitable for drug delivery. Furthermore, dramatic changes in size distribution were observed in all three nanocomplexes at acidic pH from sub-hundred nanometers to approximately 200 nm, owing to three possible explanations: 1) at acidic pH, boronic ester becomes labile, and DOX is easily released from the hydrophobic core of the nanocomplex; 2) the solubility of DOX is significantly increased at acidic pH because of the protonation of the amine moiety; and 3) the hydrophobicity of pPBA is increased by the protonation of carboxylic acid on the hydrolyzed pMA backbone, as inferred from the decreased size in acidic condition in Figure S5A.

pPBA-DOX nanocomplexes were designed for the effective delivery of DOX by passive targeting from the EPR effect and active targeting from residual PBA moieties. The cytotoxicity of the nanocomplexes was significantly higher than that of the

DOX *in vitro*, possibly as a result of the suitable size for uptake and targeting. To verify the targeting effect by the residual PBA of nanocomplexes 2 and 4, a ligand competitive assay was designed as follows. Free PBA was pre-treated to occupy the sialylated epitope to inhibit the PBA-mediated uptake of the nanocomplexes. No significant differences were observed from the cytotoxicity of nanocomplex 1, regardless of the existence of pre-treatment, thus suggesting that no additional PBA moieties could be utilized as targeting ligands after the formulation of the nanocomplexes. Moreover, a significant inhibition of cytotoxicity was observed from nanocomplexes 2 and 4 pre-treated with ligands. Similar results were obtained by confocal microscopy, thus demonstrating the function of ligand-mediated uptake *via* the PBA moiety and the sialylated epitope in cancer cells. Additionally, the importance of nano-sized structures in cellular uptake was verified by confocal microscopy.

In this study, pPBA-DOX nanocomplexes with a high molar ratio of pPBA were designed to enhance the targeting effect by residual PBA moieties. Moreover, the formation of specific structures has been revealed to be an important factor for successful cellular uptake. Therefore, the efficient delivery of nanocomplexes *in vivo* was expected. To ensure blood compatibility after introduction *in vivo*, hemolysis of the nanocomplexes was evaluated. Because of the positive charge and strong hydrophobicity of DOX, a certain level of hemolysis was induced by free DOX. However, none of the pPBA materials exhibited hemolysis because of their negative charge.

For the next step, the biodistribution of the nanocomplexes was monitored by fluorescence imaging to confirm the *in vivo* targeting effect. The accumulation of nanocomplexes was significantly enhanced as the amount of residual pPBA increased. Quantification by average epifluorescence of the tumor site showed that nanocomplex 4 exhibited a 2.5-fold stronger signal in comparison with nanocomplex 1. Although an equal amount of pPBA (4 mmol/L) was injected, interestingly, relatively low tumor accumulation was observed in the pPBA-injected mice compared with those injected with nanocomplex 4. Instead, most of the fluorescence signal from pPBA-injected mice was observed at the kidney rather than at the tumor site. Similarly, *ex vivo* images of each tumor showed a significant contrast in the epifluorescence due to the different targeting abilities of the three nanocomplexes. These results indicate that 1) free pPBA is secreted, 2) accumulation at the tumor site requires the formation of certain structures, and 3) accumulation at the tumor site can be enhanced by an additional targeting ligand.

As mentioned above, the formation of nanocomplexes enabled the successful accumulation at the tumor site *in vivo* through both passive targeting from the EPR effect and active targeting from the residual PBA moieties. Moreover, the nanocomplexes exhibited an excellent anti-cancer effect *in vitro*. Overall, the results from the *in vitro* study and the *in vivo* biodistribution strongly suggest the potential of the nanocomplexes as an efficient anti-tumor agent. From our anti-tumor study *in vivo*, the tendency of tumor growth between saline- and pPBA-injected mice was similar, thereby indicating that pPBA itself had no therapeutic effect. Because DOX itself is a practical anti-cancer drug, a certain level of anti-tumor activity was observed. However, the systemic administration of DOX still carries the risk of systemic toxicity, owing to the hemolytic property, as demonstrated by the hemolysis assays, and the possibility of non-specific delivery. The tumor growth observed in mice treated with nanocomplex 1 was similar to that in mice treated with free DOX. As expected, nanocomplexes 2 and 4 exhibited the most significant anti-tumor effect compared with the other samples. These results can be explained by the advantages of precisely designed pPBA-DOX nanocomplexes described above: 1) extended blood circulation time due to strong negative charge, 2) successful accumulation at the tumor site from both the EPR effect and targeting effect, 3) enhanced uptake, owing to the existence of residual PBA moieties, and 4) successful intracellular pH-responsive DOX release after uptake. Similar results were obtained by the luciferase assay of grown tumors, thus suggesting the anti-tumor effect of the nanocomplexes at the histological level. In addition, the changes in the body weights of all sample-treated mice indicated that none of the samples induced severe systemic toxicity at the administered doses.

In conclusion, whereas most of the previously designed DOX delivery vehicles have been focused on charge interaction or hydrophobic interaction, our approach takes advantage of a different phenomenon, the specific formation of a boronic ester between the 1,3-diol of DOX and the phenylboronic acid of pPBA. Despite its ease of preparation, our pPBA-DOX nanocomplex exhibited strong anti-tumor effect both *in vitro* and *in vivo*. The improved therapeutic effect of the nanocomplexes can be explained by tumor targeting *via* the EPR effect, active targeting via the enhanced cellular uptake by residual PBA moieties, and cargo release in the intracellular environment. Together, the overall results from the *in vitro* and *in vivo* studies suggest promising therapeutic potential of pPBA-DOX nanocomplexes in biomedical applications.

Acknowledgements

This research was supported by the Institute for Basic Science (IBS) in Korea (No IBS-R007-G2).

Author contribution

Junseok LEE performed most of the experiments and wrote the draft of the manuscript; Jinhwan KIM designed the overall experiment and wrote the draft of the manuscript; Junseok LEE, Jinhwan KIM, Yeong Mi LEE, and Sooseok IM participated in the animal experiments; Dongsik PARK contributed to the experimental part of the physicochemical characterization; Eun Ho SONG contributed to the chemical synthesis; Hansoo PARK contributed to the experimental design, and provided invaluable guidance; Won Jong KIM supervised the overall project and wrote the manuscript, to which all other authors contributed.

Supplementary information

Supplementary information is available at the website of Acta Pharmacologica Sinica.

References

1 Whitesides GM, Grzybowski B. Self-assembly at all scales. Science 2002; 295: 2418–21.
2 Bishop KJM, Wilmer CE, Soh S, Grzybowski BA. Nanoscale forces and their uses in self-assembly. Small 2009; 5: 1600–30.
3 Chandler D. Interfaces and the driving force of hydrophobic assembly. Nature 2005; 437: 640–47.
4 Faul CFJ, Antonietti M. Ionic self-assembly: facile synthesis of supramolecular materials. Adv Mater 2003; 15: 673–83.
5 Antonietti M, Forster S. Vesicles and liposomes: a self-assembly principle beyond lipids. Adv Mater 2003; 15: 1323–33.
6 Bae Y, Fukushima S, Harada A, Kataoka K. Design of environment-sensitive supramolecular assemblies for intracellular drug delivery: Polymeric micelles that are responsive to intracellular pH change. Angew Chem Int Edit 2003; 42: 4640–43.
7 Kataoka K, Harada A, Nagasaki Y. Block copolymer micelles for drug delivery: design, characterization and biological significance. Adv Drug Deliver Rev 2012; 64: 37–48.
8 Rosler A, Vandermeulen GW, Klok HA. Advanced drug delivery devices via self-assembly of amphiphilic block copolymers. Adv Drug Deliver Rev 2012; 64: 270–9.
9 Allen TM, Cullis PR. Drug delivery systems: entering the mainstream. Science 2004; 303: 1818–22.
10 Maeda H. The enhanced permeability and retention (EPR) effect in tumor vasculature: the key role of tumor-selective macromolecular drug targeting. Adv Enzyme Regul 2001; 41: 189–207.
11 Cho KJ, Wang X, Nie SM, Chen Z, Shin DM. Therapeutic nanoparticles for drug delivery in cancer. Clin Cancer Res 2008; 14: 1310–6.
12 Torchilin V. Tumor delivery of macromolecular drugs based on the EPR effect. Adv Drug Deliver Rev 2011; 63: 131–5.
13 Maeda H, Wu J, Sawa T, Matsumura Y, Hori K. Tumor vascular permeability and the EPR effect in macromolecular therapeutics: a review. J Control Release 2000; 65: 271–84.
14 Allen TM, Cullis PR. Liposomal drug delivery systems: from concept to clinical applications. Adv Drug Deliver Rev 2013; 65: 36–48.
15 Jeon H, Kim J, Lee YM, Kim J, Choi HW, Lee J, *et al*. Poly-paclitaxel/cyclodextrin-SPION nano-assembly for magnetically guided drug delivery system. J Control Release 2016; 231: 68–76.
16 Meng FH, Zhong ZY, Feijen J. Stimuli-responsive polymersomes for programmed drug delivery. Biomacromolecules 2009; 10: 197–209.
17 Kim J, Lee YM, Kang Y, Kim WJ. Tumor-homing, size-tunable clustered nanoparticles for anticancer therapeutics. ACS Nano 2014; 8: 9358–67.
18 Saravanakumar G, Lee J, Kim J, Kim WJ. Visible light-induced singlet oxygen-mediated intracellular disassembly of polymeric micelles co-loaded with a photosensitizer and an anticancer drug for enhanced photodynamic therapy. Chem Commun 2015; 51: 9995–98.
19 Kuerer HM, Newman LA, Smith TL, Ames FC, Hunt KK, Dhingra K, *et al*. Clinical course of breast cancer patients with complete pathologic primary tumor and axillary lymph node response to doxorubicin-based neoadjuvant chemotherapy. J Clin Oncol 1999; 17: 460–9.
20 Tacar O, Sriamornsak P, Dass CR. Doxorubicin: an update on anti-cancer molecular action, toxicity and novel drug delivery systems. J Pharm Pharmacol 2013; 65: 157–70.
21 Friesen C, Herr I, Krammer PH, Debatin KM. Involvement of the CD95 (APO-1/Fas) receptor/ligand system in drug-induced apoptosis in leukemia cells. Nat Med 1996; 2: 574–77.
22 Muggia FM, Hainsworth JD, Jeffers S, Miller P, Groshen S, Tan M, *et al*. Phase II study of liposomal doxorubicin in refractory ovarian cancer: antitumor activity and toxicity modification by liposomal encapsulation. J Clin Oncol 1997; 15: 987–93.
23 Ahmed F, Pakunlu RI, Brannan A, Bates F, Minko T, Discher DE. Biodegradable polymersomes loaded with both paclitaxel and doxorubicin permeate and shrink tumors, inducing apoptosis in proportion to accumulated drug. J Control Release 2006; 116: 150–8.
24 Kim D, Lee ES, Park K, Kwon IC, Bae YH. Doxorubicin loaded pH-sensitive micelle: antitumoral efficacy against ovarian A2780/DOX(R) tumor. Pharm Res-Dord 2008; 25: 2074–82.
25 Shuai XT, Ai H, Nasongkla N, Kim S, Gao JM. Micellar carriers based on block copolymers of poly(e-caprolactone) and poly(ethylene glycol) for doxorubicin delivery. J Control Release 2004; 98: 415–26.
26 Barenholz Y. Doxil (R) — The first FDA-approved nano-drug: lessons learned. J Control Release 2012; 160: 117–34.
27 Gabizon A, Shmeeda H, Barenholz Y. Pharmacokinetics of pegylated liposomal doxorubicin — Review of animal and human studies. Clin Pharmacokinet 2003; 42: 419–36.
28 Gabizon A, Catane R, Uziely B, Kaufman B, Safra T, Cohen R, *et al*. Prolonged circulation time and enhanced accumulation in malignant exudates of doxorubicin encapsulated in polyethylene-glycol coated liposomes. Cancer Res 1994; 54: 987–92.
29 Batist G, Ramakrishnan G, Rao CS, Chandrasekharan A, Gutheil J, Guthrie T, *et al*. Reduced cardiotoxicity and preserved antitumor efficacy of liposome-encapsulated doxorubicin and cyclophosphamide compared with conventional doxorubicin and cyclophosphamide in a randomized, multicenter trial of metastatic breast cancer. J Clin Oncol 2001; 19: 1444–54.
30 Zhang LF, Granick S. How to stabilize phospholipid liposomes (using nanoparticles). Nano Lett 2006; 6: 694–8.
31 Torchilin VP. Micellar nanocarriers: pharmaceutical perspectives. Pharm Res-Dord 2007; 24: 1–16.
32 Zhang L, Gu FX, Chan JM, Wang AZ, Langer RS, Farokhzad OC. Nanoparticles in medicine: therapeutic applications and developments. Clin Pharmacol Ther 2008; 83: 761–9.
33 Park H, Park W, Na K. Doxorubicin loaded singlet-oxygen producible polymeric micelle based on chlorine e6 conjugated pluronic F127 for overcoming drug resistance in cancer. Biomaterials 2014; 35: 7963–9.
34 Lee J, Jeong C, Kim, WJ. Facile fabrication and application of near-IR light-responsive drug release system based on gold nanorods and phase change material. J Mater Chem B 2014; 2: 8338–45.
35 Li L, ten Hagen TL, Hossann M, Suss R, van Rhoon GC, Eggermont AMM, *et al*. Mild hyperthermia triggered doxorubicin release from optimized stealth thermosensitive liposomes improves intratumoral drug delivery and efficacy. J Control Release 2013; 168: 142–50.
36 Lee J, Park H, Kim WJ. Nano “Chocolate Waffle” for near-IR responsive drug releasing system. Small 2015; 11: 5315–23.
37 Duan XP, Xiao JS, Yin Q, Zhang ZW, Yu HJ, Mao SR, *et al*. Smart pH-sensitive and temporal-controlled polymeric micelles for effective combination therapy of doxorubicin and disulfiram. ACS Nano 2013; 7: 5858–69.
38 Bagalkot V, Farokhzad OC, Langer R, Jon S. An aptamer-doxorubicin physical conjugate as a novel targeted drug-delivery platform. Angew Chem Int Edit 2006; 45: 8149–52.
39 Liu FY, He XX, Lei Z, Liu L, Zhang JP, You HP, *et al*. Facile Preparation of doxorubicin-loaded upconversion@polydopamine nanoplatforms for simultaneous *in vivo* multimodality imaging and chemophotothermal synergistic therapy. Adv Healthc Mater 2015; 4: 559–68.

40 Kim H, Lee D, Kim J, Kim TI, Kim WJ. Photothermally triggered cytosolic drug delivery via endosome disruption using a functionalized reduced graphene oxide. ACS Nano 2013; 7: 6735–46.
41 Liu Z, Fan AC, Rakhra K, Sherlock S, Goodwin A, Chen XY, *et al*. Supramolecular stacking of doxorubicin on carbon nanotubes for *in vivo* cancer therapy. Angew Chem Int Edit 2009; 48: 7668–72.
42 Meng HA, Liong M, Xia TA, Li ZX, Ji ZX, Zink JI, *et al*. Engineered design of mesoporous silica nanoparticles to deliver doxorubicin and P-glycoprotein siRNA to overcome drug resistance in a cancer cell line. ACS Nano 2010; 4: 4539–50.
43 Manocha B, Margaritis A. Controlled release of doxorubicin from doxorubicin/gamma-polyglutamic acid ionic complex. J Nanomater 2010; 2010: 780171.
44 Kuivila HG, Keough AH, Soboczenski EJ. Areneboronates from diols and polyols. J Org Chem 1954; 19: 780–3.
45 Yang WQ, Gao XM, Wang BH. Boronic acid compounds as potential pharmaceutical agents. Med Res Rev 2003; 23: 346–68.
46 Yan J, Springsteen G, Deeter S, Wang BH. The relationship among pK(a), pH, and binding constants in the interactions between boronic acids and diols — it is not as simple as it appears. Tetrahedron 2004; 60: 11205–9.
47 Li YP, Xiao WW, Xiao K, Berti L, Luo JT, Tseng HP, *et al*. Well-defined, reversible boronate crosslinked nanocarriers for targeted drug delivery in response to acidic pH values and *cis*-Diols. Angew Chem Int Edit 2012; 51: 2864–9.
48 Kim J, Lee YM, Kim H, Park D, Kim J, Kim WJ. Phenylboronic acid-sugar grafted polymer architecture as a dual stimuli-responsive gene carrier for targeted anti-angiogenic tumor therapy. Biomaterials 2016; 75: 102–11.
49 Ceglowski M, Gierczyk B, Schroeder G. Poly(methyl vinyl ether-alt-maleic anhydride) functionalized with 3-aminophenylboronic acid: a new boronic acid polymer for sensing diols in neutral water. J Appl Polym Sci 2014; 131: 40778.
50 Jeong JH, Byoun YS, Lee YS. Poly(styrene-alt-maleic anhydride)-4-aminophenol conjugate: synthesis and antibacterial activity. React Funct Polym 2002; 50: 257–63.
51 Dube; DH, Bertozzi CR. Glycans in cancer and inflammation. Potential for therapeutics and diagnostics. Nat Rev Drug Discov 2005; 4: 477–88.
52 Djanashvili K, Frullano L, Peters JA. Molecular recognition of sialic acid end groups by phenylboronates. Chemistry 2005; 11: 4010–8.
53 Deshayes S, Cabral H, Ishii T, Miura Y, Kobayashi S, Yamashita T, *et al*. Phenylboronic acid-installed polymeric micelles for targeting sialylated epitopes in solid tumors. J Am Chem Soc 2013; 135: 15501–7.